ISSN: 2472-3703 DOI: 10.6911/WSRJ.202312_9(12).0004

The Study of the Impact of Bowl Oversize on the Cleaning of 825 Nickel-based Alloy Bimetallic Pipes

Yang Wang[1], Yue Gao[1], Lan Tang[1], Jian Yang[1], Zheyi Jin[2], Weiye Zhuang [2], Yujia Li[2] and Tao Ren[3]

[1]PetroChina Southwest Oil & gas field northeast gas field, Dazhou, China

[2]Southwest Petroleum University, Chengdu, China

[3]Chengdu University of Technology, Chengdu, China

Abstract

With the development of high-sulfur oil and gas fields and the application of gas-liquid mixed transportation processes, ordinary carbon steel pipelines are unable to meet the production requirements of high-sulfur oil and gas fields due to their poor corrosion resistance. Bimetallic composite pipes, which use carbon steel as the outer pipe and corrosion-resistant alloy as the inner liner, have been developed and applied to effectively solve the problem of pipeline corrosion. However, the inner liner of bimetallic composite pipes is relatively soft, and the extent of wear and damage caused by existing cleaning methods for carbon steel pipes on composite pipes is not yet clear. In response to the above issues, this study selects and investigates the constitutive model of polyurethane rubber, theoretically calculates the stress conditions of the pipe in the pipeline, and uses Finite Element Analysis simulation to analyze the cleaning effect of the pipe impurities based on the shape of the cleaning tool, excess clearance, and operating speed.

Keywords

Pipe cleaner; Bimetallic composite pipes; Simulation analysis; Frictional wear.

1. INTRODUCTION

With the deepening development of high-sulfur gas mines in various regions, the content of strong corrosive media such as H2S, CO2, Cl- in the produced gas is increasing. Ordinary carbon steel pipelines are unable to meet the production requirements of high-sulfur oil and gas fields due to their poor corrosion resistance. It has been proven that bimetallic composite pipes, which use carbon steel as the outer pipe and corrosion-resistant alloy as the inner liner, not only ensure the normal operation of the pipeline but also reduce the construction cost, making it an effective solution to the problem of pipeline corrosion.

Bimetallic composite pipes are formed by a special process that combines two different materials. According to the method of combining the inner and outer pipes, they can be divided into mechanical composite and metallurgical composite. Mechanical composite is mainly achieved by mechanically reducing the diameter of the inner liner and outer pipe simultaneously to achieve their combination. The advantages of this method are convenient operation and efficient production, but the disadvantage is that the combination between the inner liner and outer pipe is not tight, and delamination may occur at high temperatures. Metallurgical composite can be further divided into fusion bonding and diffusion bonding. Fusion bonding refers to the melting and mixing of the inner and outer pipes at high temperatures, followed by solidification to achieve a tight combination. Diffusion bonding, on

ISSN: 2472-3703 DOI: 10.6911/WSRJ.202312_9(12).0004

the other hand, involves significant plastic deformation of the inner and outer materials at higher temperatures, allowing the metal to diffuse across the interface and bond the inner liner and outer pipe[1].

Compared to foreign countries, research on bimetallic composite pipes started relatively late in China and was only applied in engineering in 1991. Since 2001, this technology has gradually been applied, mainly to add inner liners to ordinary pipelines that have failed after long-term use in order to achieve their intended use again. In 2005, during the modification and alteration of gas production and gathering pipelines in the Tarim Basin gas field in Xinjiang[2]，[3], a bimetallic composite pipe was designed and applied, which consisted of a 20# boiler steel outer pipe and a 316L austenitic stainless steel inner liner. This pipeline solved the corrosion problems of the inner liner and welds.

2. SELECTION AND EXPERIMENTAL STUDY OF POLYURETHANE RUBBER CONSTITUTIVE MODEL FOR CLEANING TOOL SKIN BOWL MATERIAL

Establishing the correct constitutive model of the cleaning tool skin bowl material is an important prerequisite for theoretical analysis and experimental research on cleaning tool cleaning. The material of the cleaning tool skin bowl is mainly polyurethane rubber. Polyurethane rubber material has super elasticity and excellent flexibility. In recent years, the research on rubber materials generally uses the models shown in Table 1. In this study, uniaxial tensile tests were conducted on polyurethane rubber of the cleaning tool skin bowl, and the constitutive model of the polyurethane rubber of the cleaning tool skin bowl was determined through fitting.

Table 1. Characteristics and Applicability of Three Models

Constitutive Model	Characteristics and Applicability Range
Mooney-Rivlin Model	Suitable for small and medium deformations, but cannot accurately simulate rubber with added carbon black
Yeoh Model	Can describe the filled rubber after adding carbon black, but cannot accurately describe the situation of small deformation
Ogden Model	There is no essential difference from the Mooney-Rivlin model

This study mainly focuses on the deformation of unfilled rubber materials, so the Mooney-Rivlin model was chosen for research and analysis. Assuming isotropy and incompressibility of the rubber material, the constitutive model of the rubber material is established based on the stress-strain relationship. According to the strain energy function of the Mooney-Rivlin model [4], the strain energy can be decomposed into strain deviation energy and volumetric strain energy. After Taylor expansion, Equation (1-1) is obtained.

$$U = \sum_{i+j=1}^{N} C_{ij}(I_1 - 3)^i(I_2 - 3)^j + \sum_{i=1}^{N} \frac{1}{D_i}(J - 1)^{2i} \qquad (1-1)$$

In the equation, $C_{ij}$to obtain the coefficients for the expansion, i，jTake values of either 0 or 1 separately, These coefficients represent the constitutive model coefficients for polyurethane material, which need to be obtained through tensile experiments.; D_i is the model constant; N is the polynomial order.

ISSN: 2472-3703 DOI: 10.6911/WSRJ.202312_9(12).0004

To obtain the appropriate parameters for the polyurethane hyperelastic constitutive model, uniaxial tensile tests were conducted on the polyurethane elastic material. The experimental equipment used was the WDW series electronic universal testing machine, as shown in Figure 1 (a). The chosen material for the experiment is polyurethane rubber with a hardness of 90A. Tensile test specimens were fabricated according to the standard GB_T 1040.2-2006[5], with a thickness of 3mm, and the specimen dimensions are as shown in Figure 1 (b). The material stress-strain curve is obtained as shown in Figure1(c). Experimental data points were selected for linear fitting, resulting in the fitted curve as shown in Figure1(d), C_{10}=0.7029, C_{01}=0.5262.

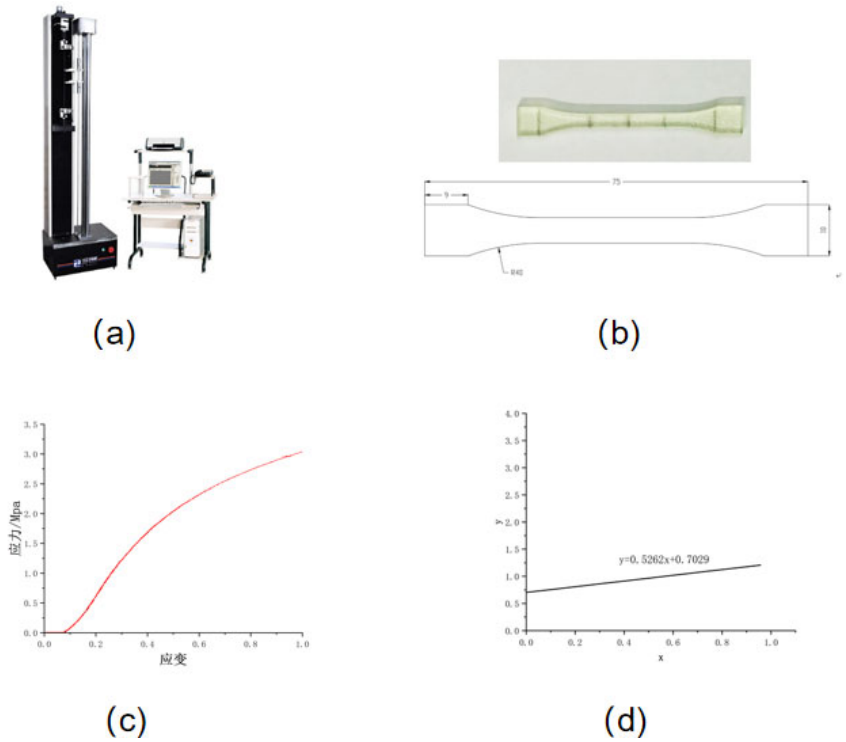

Figure 1. (a) WDW Series Electronic Universal Testing Machine, (b) Specimen and Specimen Dimensions, (c) Stress-Strain Curve of Polyurethane, (d) Linear Fit of the Mooney-Rivlin Model.

To validate the accuracy of the Mooney-Rivlin model in fitting the constitutive behavior of polyurethane, finite element analysis was performed on polyurethane specimens. The experimentally measured C_{10} 、 C_{01} were used as input. The mesh was refined in the polyurethane region primarily subjected to deformation, utilizing hexahedral C3D8H elements, as shown in Figure 2(a). Based on the actual conditions of the polyurethane tensile test, a fully fixed constraint was applied to the left end of the polyurethane, and a displacement load was applied to the right end with a magnitude of 20mm.The finite element simulation resulted in a Mises stress distribution map of the polyurethane rubber, as depicted in Figure2(b). The stress magnitude distribution from the analysis closely matched the actual loading trend of the polyurethane specimen. This indicates that the Mooney-Rivlin model parameters C_{10}、C_{10} obtained from the experiment are reasonably accurate.

ISSN: 2472-3703 DOI: 10.6911/WSRJ.202312_9(12).0004

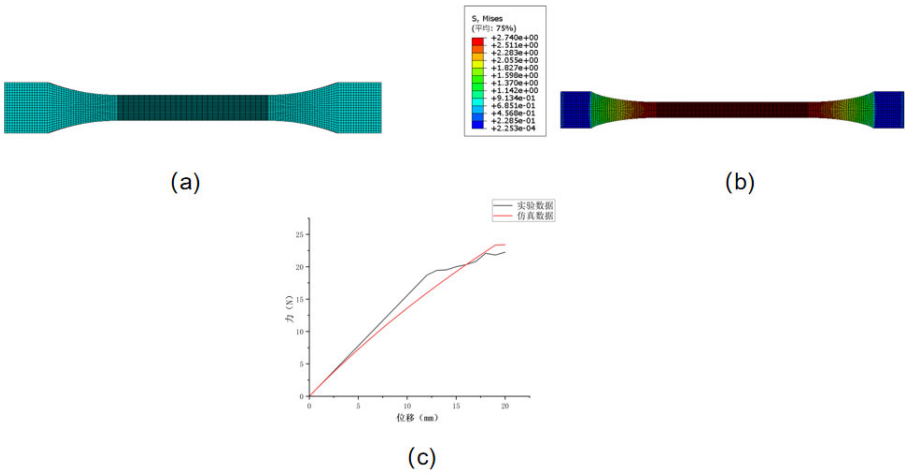

Figure 2. (a) Mesh Division of Polyurethane Rubber, (b) Stress Contour Map of Polyurethane Obtained Using Mooney-Rivlin Model, (c) Force-Displacement Curve of Polyurethane Deformation Obtained from Experiment and Finite Element Simulation.

3. THE STUDY OF THE PHYSICAL PROCESS OF CLEANING DEVICES FOR REMOVING IMPURITIES

3.1. A physical model for impurity layer delamination

In general, when the hardness of the cleaning device is greater than that of the impurities, effective cleaning can be achieved. Given that pipes, the impurity layer, and the cleaning device exhibit axial symmetry, a two-dimensional physical model can be established. Taking into account the flexibility of the cleaning device's scraper, a model for the delamination of the impurity layer during cleaning operations is shown in Figure 3. The entire impurity region can be divided into three parts: the undamaged impurity layer zone, the plastic deformation zone, and the impurity debris zone. As the cleaning device moves, the plastic deformation zone gradually evolves into impurity debris and detaches from the surface of the cleaning device[6].

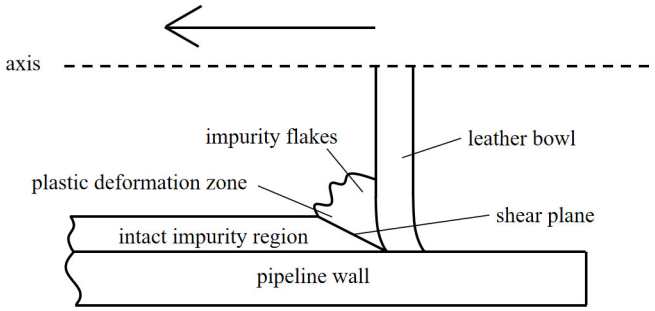

Figure 3. Physical Model of Impurity Layer Delamination.

3.2. The slip field within the plastic deformation zone

The problem of impurity layer delamination during pipe cleaning is not only a mechanical issue but also a kinematic one. Therefore, the relevant analysis should simultaneously satisfy the requirements of both mechanics and kinematics. Assuming the scraping bowl's operating speed is $-v$, based on the principle of relativity, we can transform this scenario into one where the scraping bowl is stationary, and the pipe wall and impurity layer are moving at a speed of v. As shown in Figure 4, we assume the thickness of the undamaged impurity layer to be δ_w , and the average thickness of impurity debris above the AB boundary to be δ_w'. A perpendicular line drawn through A to line OB results in AC, yielding $\delta_w' = |AC|$.

ISSN: 2472-3703 DOI: 10.6911/WSRJ.202312_9(12).0004

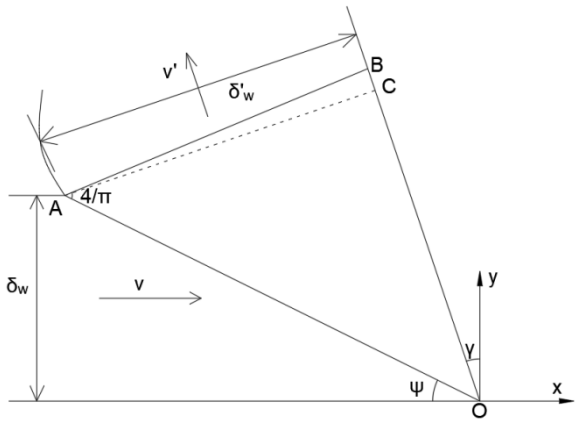

Figure 4. Schematic Diagram of Velocity and Thickness During Impurity Layer Delamination Process.

In the diagram, γ represents the inclination angle of the scraping bowl. By geometric relationships, $\delta'_w = (\cot\varphi\cos\gamma - \sin\gamma)\delta_w$ can be determined, and the average velocity of impurity debris above AB is

$$v' = \frac{v}{\cot\varphi\cos\gamma - \sin\gamma} \qquad (2-1)$$

As shown in Figure 5, starting from the origin point O with a horizontal velocity v, representing the velocity of the rigid region on the left side of OA . Draw a segmented velocity line parallel to OA from point $o'a'$, where point a' is unknown, and the length of line segment $o'a' - a'$ represents the velocity difference between the plastic region on the right side of OA and the rigid region on the left side.

Because after point a', there is another segment in the direction of AB, exactly representing the velocity of the rigid region above the AB interface, draw a line segment $a' - a'b'$ parallel to AB from point a'. The segment $a' - a'b'$ represents the velocity difference between the plastic regions and the rigid regions on both sides of the AB interface. Connecting $o - a'b'$ completes the velocity vector diagram.

If $o - a'b'$ is parallel to the boundary OB, it indicates that the slip line field satisfies the boundary velocity conditions, and the impurity debris above AB slides along the interface OB direction.

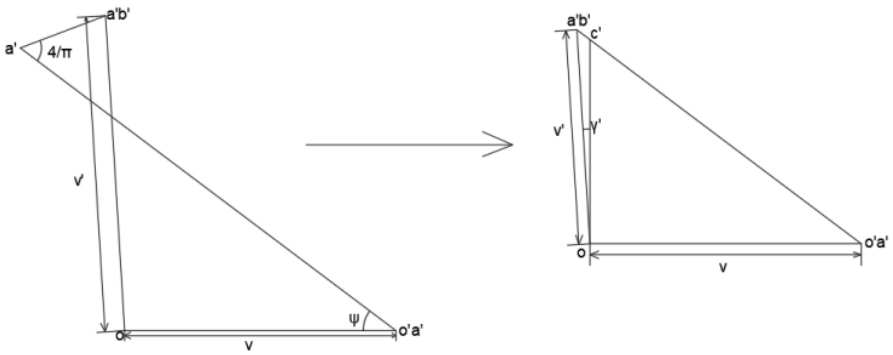

Figure 5. Velocity Vector Diagram of Impurity Layer Delamination

Based on the Law of Sines and geometric relationships, we can derive.

ISSN: 2472-3703 DOI: 10.6911/WSRJ.202312_9(12).0004

Based on the Law of Sines and geometric relationships, we can derive

$$v' = \frac{v}{\cot\varphi \cos\gamma' - \sin\gamma'} \qquad (2-2)$$

Comparing equations (3-1) and (3-2), it can be observed that $\gamma' = \gamma$. Consequently, $o - a'b'$ is parallel to OB, indicating that the slip line field satisfies the boundary velocity conditions, and the impurity debris above AB slides along the interface OB direction.

4. CONTACT MECHANICS ANALYSIS OF CLEANER IN BIMETALLIC COMPOSITE PIPE

To analyze the contact mechanics characteristics between the cleaner and the 825 nickel-based alloy, and further determine whether the cleaner will cause the failure of the 825 nickel-based alloy lining of the bimetallic composite pipe during the cleaning operation, finite element analysis software is now used to separately establish The models of three shapes of cleaners, namely bowl-shaped, flat-plate-shaped and spherical, running inside the bimetallic composite pipe under the condition of no impurities. The simplified geometric models of the three are shown in Figure 6, and the parameters of the oversize condition are shown in Table 6 This article selects the 825 nickel-based alloy lining of the bimetallic composite pipe as the research object. The length of the pipe used is $L_c = 500\text{mm}$, the inner diameter is $D_e = 295\text{mm}$, and the outer diameter is $D_c = 301\text{mm}$.

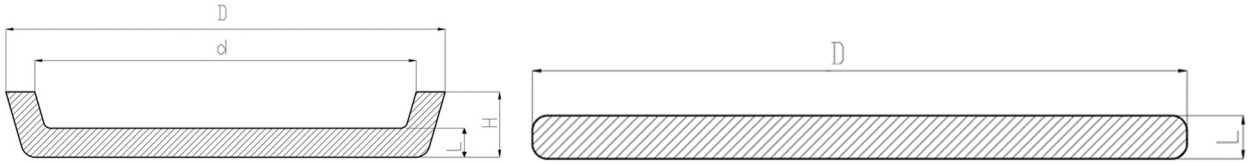

(a) Schematic diagram of bowl-shaped cleaner (b) Schematic diagram of flat-plate cleaner

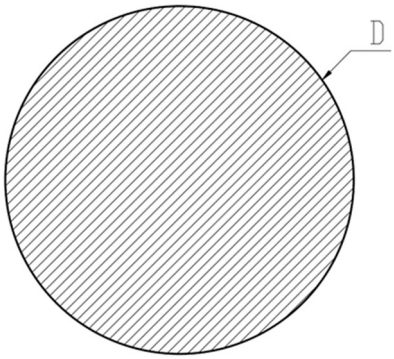

(c) Spherical Drain Cleaning Device Diagram

Figure 6. Schematic diagram of cleaner geometric model.

Table 2. Different oversize parameters

Working Condition	1	2	3	4
Oversize(%)	1	2	3	4

ISSN: 2472-3703 DOI: 10.6911/WSRJ.202312_9(12).0004

The cleaner's sealing disc material is made of superelastic material, the material parameters are set consistent with the constitutive model, and the pipe material is 825 nickel-based alloy, using a linear elastic material model, with an elastic modulus of $E = 196GPa$ and a Poisson's ratio of $\mu = 0.3$. The contact between the sealing plate and the pipe is based on the penalty function algorithm's face-to-face contact. The Coulomb friction coefficient between the sealing plate and the pipe is set to 0.4, and the normal contact is hard contact. The stainless steel pipe at both ends is fully constrained, and the cleaner's bowl moves in the direction of the pipe axis. The applied displacement load is 300mm, and a standard solver is used.

The finite element simulation is set to be conducted at 22°C. After data processing, the stress cloud diagrams of the pipe and polyurethane bowl of the bowl-shaped cleaner under different oversizes are shown in Figures7 and 8. As can be seen from the figure, when the oversize is between 1% and 4%, the maximum stresses on the pipe are 0.5826MPa, 1.33MPa, 1.985MPa, and 2.776MPa respectively; the contact stresses between the polyurethane bowl and the pipe wall are 0.0753MPa, 0.1942MPa, 0.4459MPa, and 0.2576MPa respectively. The yield strength of 825 nickel-based alloy is 423MPa, and the stress generated by the maximum oversize of the cleaner is far less than its yield strength. Therefore, when using a bowl-shaped cleaner with an oversize of 1% to 4% for cleaning operations, the 825 nickel-based alloy lining is not easy to deform during the cleaning process.

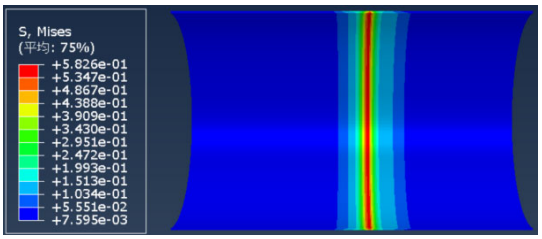

(a) Maximum stress on the pipe when the cleaner's oversize is 1%

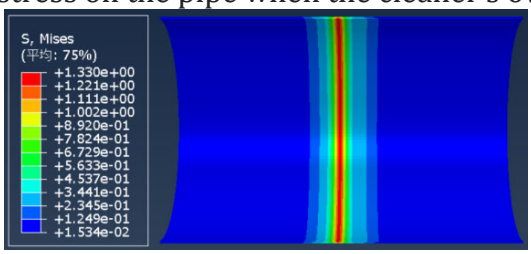

(b) Maximum stress on the pipe when the cleaner's oversize is 2%

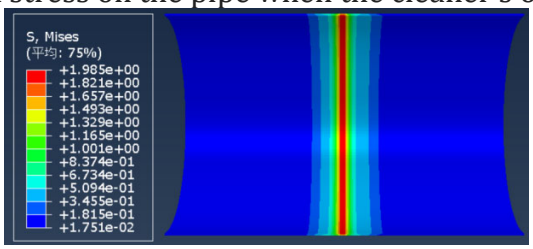

(b) Maximum stress on the pipe when the cleaner's oversize is 3%

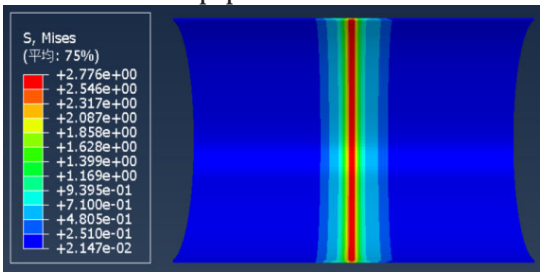

(d) Maximum stress on the pipe when the cleaner's oversize is 4%

Figure 7. Stress Cloud Diagram of the Pipe.

ISSN: 2472-3703 DOI: 10.6911/WSRJ.202312_9(12).0004

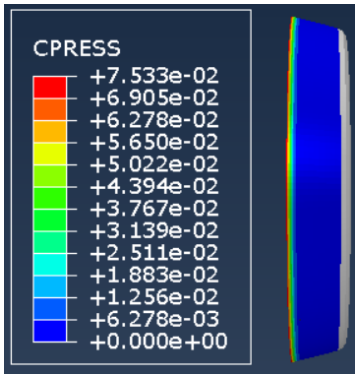

(a) Contact stress of the bowl when the oversize is 1%

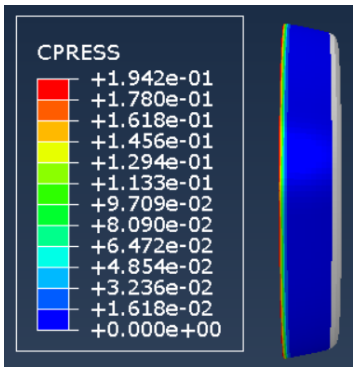

(b) Contact stress of the bowl when the oversize is 2%

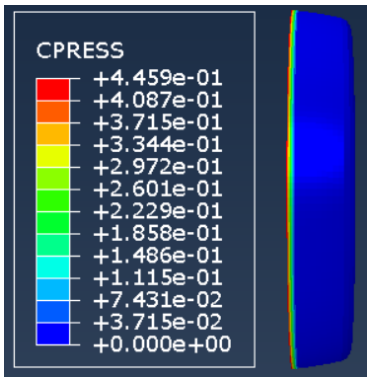

(c) Contact stress of the bowl when the oversize is 3%

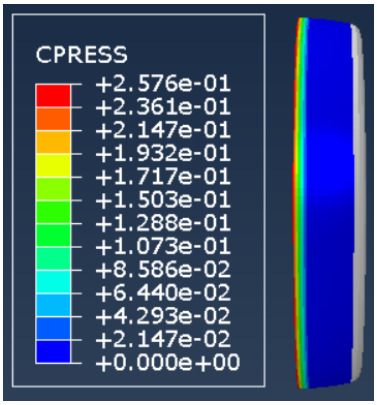

(d) Contact stress of the bowl when the oversize is 4%

Figure 8. Stress Cloud Diagram of the Polyurethane Bowl.

The stress cloud diagrams of the pipe and polyurethane of the flat-plate cleaner at different oversizes are shown in Figures 9 and 10. As can be seen from the figure, when the oversize is between 1% and 4%, the maximum stresses on the pipe are 0.6341MPa, 1.193MPa, 1.524Mpa, and 1.877Mpa respectively; the contact stresses between the polyurethane bowl and the pipe

ISSN: 2472-3703 DOI: 10.6911/WSRJ.202312_9(12).0004

wall are 0.09044Mpa, 0.09233Mpa, 0.1004Mpa, and 0.1235Mpa respectively. The yield strength of 825 nickel-based alloy is 423MPa, and the stress generated by the maximum oversize of the cleaner is far less than its yield strength. Therefore, when using a flat-plate cleaner with an oversize of 1% to 4% for cleaning operations, the 825 nickel-based alloy lining is not easy to deform during the cleaning process.

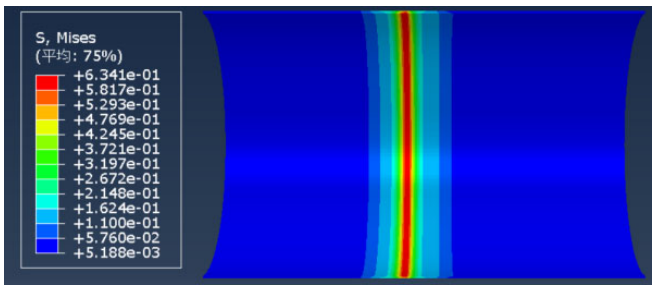

(a) Maximum stress on the pipe when the cleaner's oversize is 1%

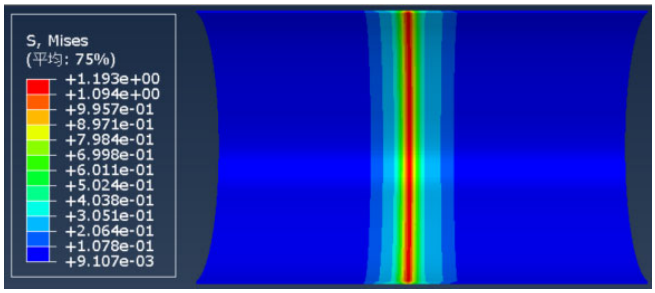

(b) Maximum stress on the pipe when the cleaner's oversize is 2%

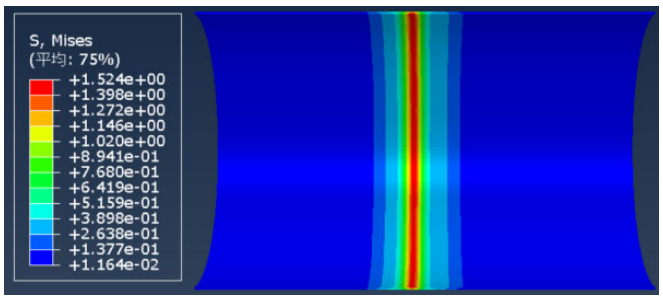

(c) Maximum stress on the pipe when the cleaner's oversize is 3%

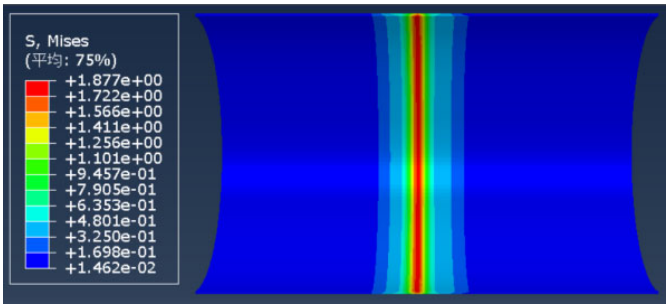

(d) Maximum stress on the pipe when the cleaner's oversize is 4%

Figure 9. Stress Cloud Diagram of the Pipe.

ISSN: 2472-3703 DOI: 10.6911/WSRJ.202312_9(12).0004

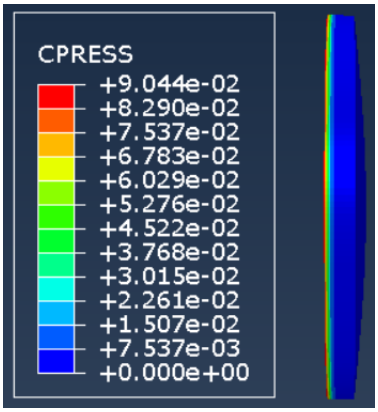

(a) Contact stress of the flat plate when the oversize is 1%

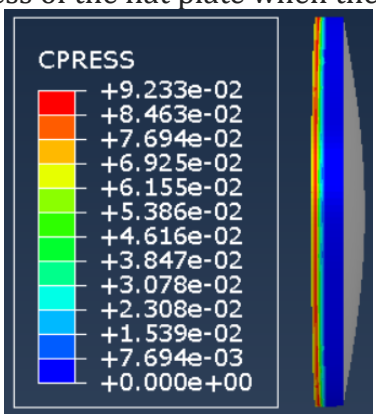

(b) Contact stress of the flat plate when the oversize is 2%

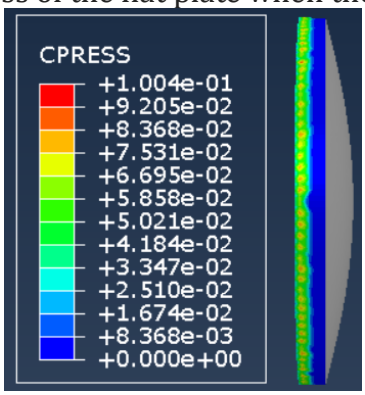

(c) Contact stress of the flat plate when the oversize is 3%

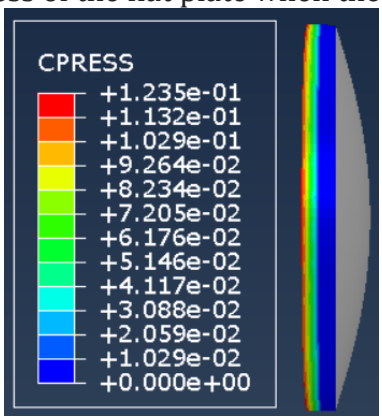

(d) Contact stress of the flat plate when the oversize is 4%

Figure 10. Stress Cloud Diagram of the Polyurethane Flat Plate.

ISSN: 2472-3703 DOI: 10.6911/WSRJ.202312_9(12).0004

The stress cloud diagrams of the pipe and polyurethane of the spherical cleaner at different oversizes are shown in Figures 11 and 12. As can be seen from the figure, when the oversize is between 1% and 4%, the maximum stresses on the pipe are 1.656Mpa, 3.027Mpa, 4.427Mpa, and 5.074Mpa respectively; the contact stresses between the polyurethane bowl and the pipe wall are 0.4024Mpa, 0.6153Mpa, 0.8034Mpa, and 1.448Mpa respectively. The yield strength of 825 nickel-based alloy is 423MPa, and the stress generated by the maximum oversize of the cleaner is far less than its yield strength. Therefore, when using a spherical cleaner with an oversize of 1% to 4% for cleaning operations, the 825 nickel-based alloy lining is not easy to deform during the cleaning process.

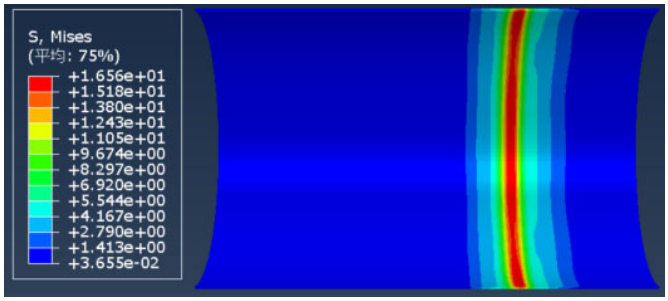

(a) Maximum stress on the pipe when the cleaner's oversize is 1%

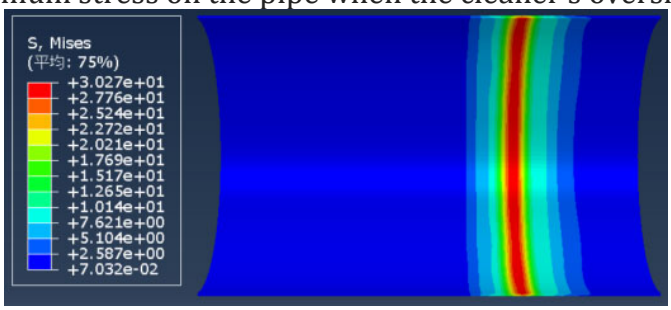

(b) Maximum stress on the pipe when the cleaner's oversize is 2%

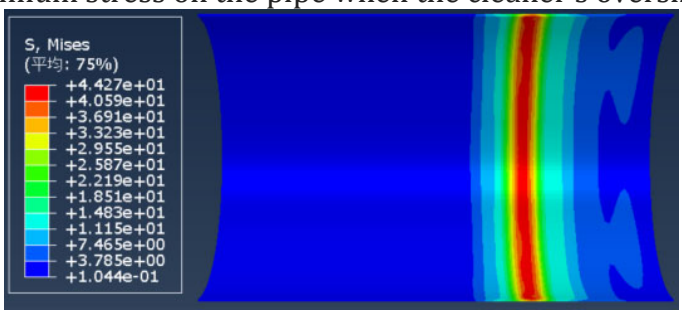

(c) Maximum stress on the pipe when the cleaner's oversize is 3%

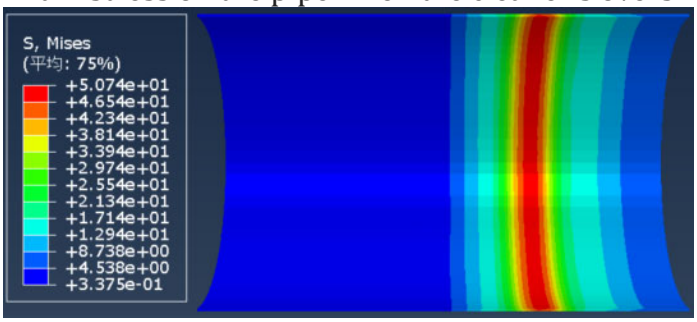

(d) Maximum stress on the pipe when the cleaner's oversize is 4%

Figure 11. Stress Cloud Diagram of the Pipe.

ISSN: 2472-3703 DOI: 10.6911/WSRJ.202312_9(12).0004

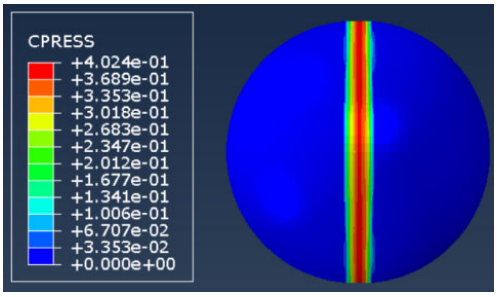

(a) Contact stress of the sphere when the oversize is 1%

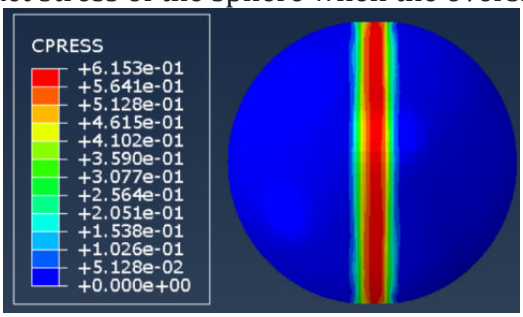

(b) Contact stress of the sphere when the oversize is 2%

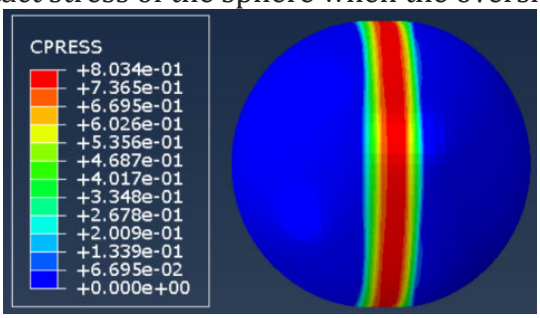

(c) Contact stress of the sphere when the oversize is 3%

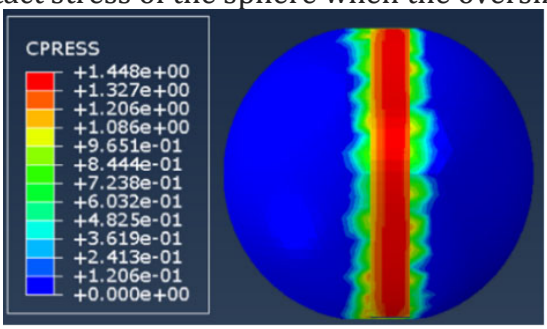

(d) Contact stress of the sphere when the oversize is 4%

Figure 12. Stress Cloud Diagram of the Spherical Polyurethane.

The comparison of the stresses received by cleaners of different shapes and oversizes and pipes is shown in Figure 13. As can be seen from Figure 13(a), when the oversize of the cleaner is 1% and 2%, the stresses received by the bowl-shaped cleaner and the flat-plate cleaner in the pipe are basically the same; when the oversize of the cleaner is 3% and 4%, the stress received by the bowl-shaped cleaner in the pipe is greater than that of the flat-plate cleaner; The stress received by the spherical cleaner in the pipe at an oversize of 1% to 4% is far greater than the other two. As can be seen from Figure 13(b), the contact stress between the bowl-shaped cleaner and the pipe wall increases first and then decreases with the increase of oversize, and the contact stress between the flat-plate cleaner and the pipe wall increases with the increase of oversize; The contact stress between the spherical cleaner and the pipe wall increases with the increase of oversize. However, at the same oversize, the contact stress between the spherical

ISSN: 2472-3703 DOI: 10.6911/WSRJ.202312_9(12).0004

cleaner and the pipe wall is greater than that of the bowl-shaped cleaner and flat-plate cleaner, so the tightness between the spherical cleaner and the inner wall of the pipe is higher.

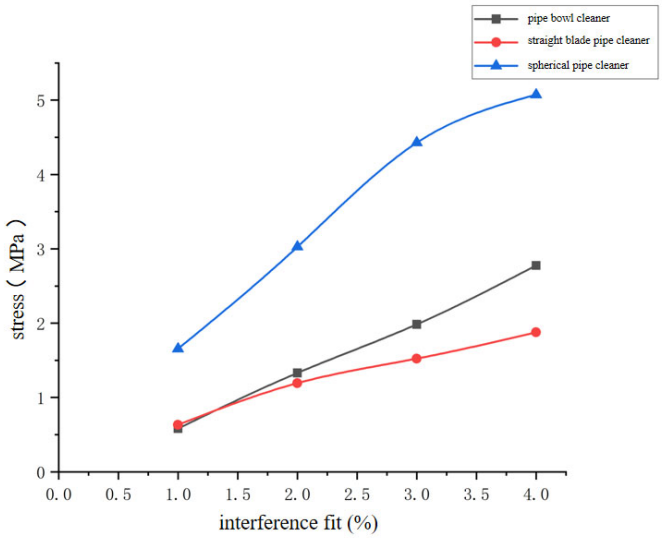

(a)Stress on the pipe during cleaning with cleaners of different shapes and oversizes

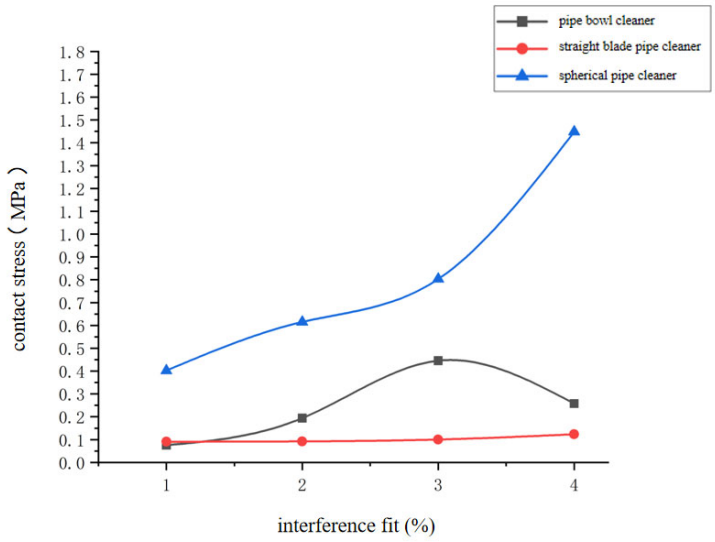

(b)Contact stress with the pipe wall for cleaners of different shapes and oversizes

Figure 13. Stress of cleaners and pipes of different shapes and oversizes.

5. FRICTION AND WEAR EXPERIMENTS OF TUBE CLEANER INTERFERENCE FIT ON PIPELINES.

Based on the simulations conducted above, it was found that in the absence of a medium, the bimetallic composite pipe does not experience liner failure during pipe cleaning operations. However, it is still unclear whether the cleaning action under this condition could cause wear on the bimetallic composite pipe, potentially leading to liner puncture. To further investigate the extent of liner wear on the bimetallic composite pipe during the cleaning process, this study will conduct a friction and wear experiment. The experiment will primarily focus on the influence of the interference fit of the cleaning tool on the polyurethane sample and 825 nickel-based alloy. This will allow an analysis of the damage to the 825 nickel-based alloy liner during the cleaning process and the changing patterns of the friction coefficient.

This article used a UMT (Universal Mechanical Tester) friction and wear testing machine for experimental testing. The dimensions of the polyurethane sample are as shown in Table 3. The

ISSN: 2472-3703 DOI: 10.6911/WSRJ.202312_9(12).0004

polyurethane sample is placed in the central position of the lower fixture, and a pressure plate is positioned on the surface of the polyurethane. The pressure plate is secured and tightened onto the lower fixture by connecting it with a nut and bolt, as illustrated in Figure 14.For the upper fixture in the experiment, the UMT friction and wear testing machine's compatible fixture is used. A 6mm diameter 825 nickel-based alloy ball is fixed onto the upper fixture.

Table 3. Polyurethane sample dimensions

parameter	length	width	thickness
dimensions（mm）	50	48	5

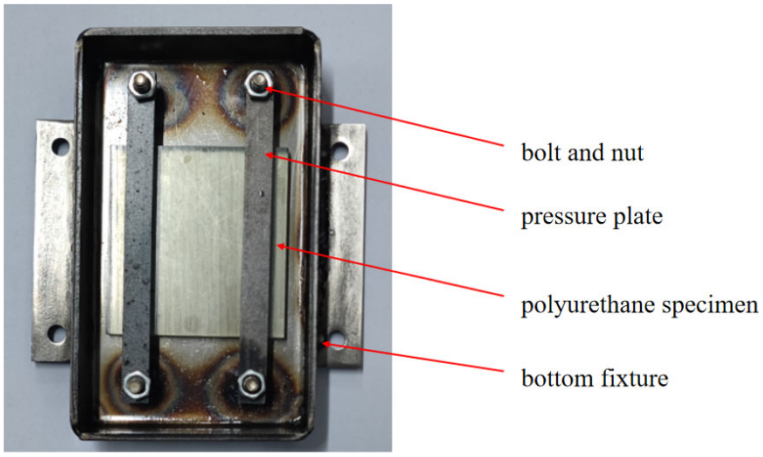

Figure 14. Assembly diagram of polyurethane test sample and lower fixture.

In order to study the friction and wear characteristics of an 825 nickel-based alloy sphere under the influence of different normal loads, experiments were conducted under dry friction conditions at room temperature (23°C). Reciprocating motion was performed at a speed of 10 mm/s with a stroke of 10 mm. Three different load conditions were established for the experiment, as shown in Table 5-2. Each individual experiment lasted for 1 hour. Data relevant to the friction and wear during the entire experiment process were collected.

Table 4. Load Settings

groups	1	2	3
load (N)	50	30	10

Due to the fact that the friction coefficient stabilizes after 100 seconds in the experiment, the time period from 0 to 100 seconds was selected for analysis. Figure 15 shows the friction coefficient curves under different normal loads.

ISSN: 2472-3703 DOI: 10.6911/WSRJ.202312_9(12).0004

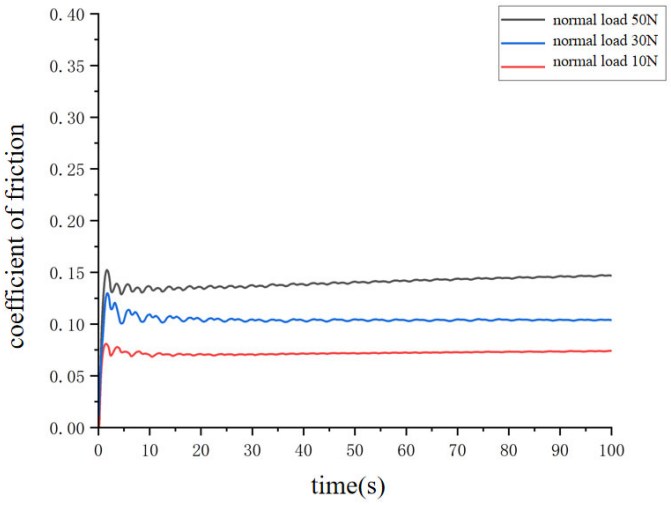

Figure 15. Friction coefficient vs. time curves under different normal loads.

From the values of the friction coefficient in the graph, from top to bottom, they represent the friction coefficients of three different load groups: 50N, 30N, and 10N. The friction coefficients for all three normal loads exhibit a sharp increase within the first 5 seconds and then rapidly decrease in the following 5 seconds. Afterward, the friction coefficients stabilize within a small range and gradually approach a steady state.During the initial 0 to 5 seconds, there is a rapid increase in the friction coefficient for the 825 nickel-based alloy sphere specimen. The main reason for this phenomenon is the relative motion between the polyurethane and the 825 nickel-based alloy sphere when the machine is started, disrupting the static equilibrium of the dry friction system, leading to a sharp increase in the friction coefficient.From 5 to 10 seconds, the friction coefficient decreases as time progresses. The specimen, driven by the motor, transitions from an accelerated motion state to a uniform motion state, resulting in a reduction in the energy input to the dry friction system and a rapid decrease in the friction coefficient. After 10 seconds, the entire dry friction coefficient remains stable.The experiment indicates that when the clearance of the tube cleaner is 4% during tube cleaning operations, it does not cause significant wear on the 825 nickel-based alloy.

All manuscripts must be in English, also the table and figure texts, otherwise we cannot publish your paper. Please keep a second copy of your manuscript in your office.

6. CONCLUSION

This paper established a simplified Mooney-Rivlin model for polyurethane deformation and used a WDW universal electronic testing machine to conduct uniaxial tensile experiments on polyurethane materials to determine the model parameters. A theoretical model for the tube cleaner in the pipeline was developed, and the entire impurity layer region was divided into three parts: the undamaged impurity layer, the plastic deformation zone, and the impurity chip zone. Furthermore, finite element analysis calculations were conducted to study the contact performance of different shapes and interference fits of the tube cleaner inside the pipeline. This research aimed to understand the impact of various tube cleaner shapes and interference fits inside the pipeline. The study indicates that in the process of tube cleaning, little to no deformation occurs in the inner lining of bimetallic composite pipes.

ISSN: 2472-3703 DOI: 10.6911/WSRJ.202312_9(12).0004

ACKNOWLEDGMENTS

This paper was supported by the Sichuan Science and Technology Program (2022YFH0119 and 2023YFH0102), the Chengdu Science and Technology Program(2022-YF05-00825-SN), and in part by the scientific starting project of SWPU(No.2021QHZ040).

REFERENCES

[1] Baoqing Zhang: A Brief Analysis of the Manufacturing Technology of Bimetallic Composite Pipes, Mechanical and Electrical Engineering Technology, Vol.38(2009) No.03, p.106-108.

[2] Yulu Sun, Zhenquan Bai, Guochao Zhang, et al: Research Status of Bimetallic Composite Pipes for Corrosion Protection in Oil and Gas Fields , Comprehensive Corrosion Control, Vol.25(2011) No.05, p.10-12+16.

[3] Li F , Wei B , Bai Z , et al: Fit for Purpose Analysis on Bimetallic Lined Pipe in Yaha Gas Condensate Field, *International Conference on Pipelines and Trenchless Technology 2011*(Beijing, China, October26-29)

[4] Qian Min: Study on the Vibration Characteristics of Two Constitutive Models for Rubber Pads Alongside Train Carriages , Machinery, Vol.42(2015) No.10, p.30-33+39.

[5] China National Standardization Management Committee. Determination of Tensile Properties of Plastics - Part 2: Test Conditions for Moulding and Extrusion Plastics: GB_T 1040.2-2006 . Beijing: China Standards Press, 2006.

[6] Weidong Li: *Research on the peeling mechanism of wax layer in crude oil pipeline pigging*. (Ph.D., China University of Petroleum, China 2019).